Solar Phys (2013) 288:55–71
DOI 10.1007/s11207-012-0113-7

Connection Between Chromospheric Events and Photospheric Dynamics

A. Anđić · J. Chae · H. Park · H. Yang · K. Ahn · W. Cao · Y.D. Park

Received: 29 June 2011 / Accepted: 20 August 2012 / Published online: 16 October 2012

Abstract We analyzed chromospheric events and their connection to oscillation phenomena and photospheric dynamics. The observations were done with the New Solar Telescope of Big Bear Solar Observatory using a broad-band imager at the wavelength of a TiO band and FISS spectrograph scanning Ca II and Hα spectral lines. The event in Ca II showed strong plasma flows and propagating waves in the chromosphere. The movement of the footpoints of flux tubes in the photosphere indicated flux tube entanglement and magnetic reconnection as a possible cause of the observed brightening and waves propagating in the chromosphere. An upward propagating train of waves was observed at the site of the downflow event in Hα. There was no clear relationship between photospheric waves and the Ca II and Hα events. Our observations indicate that chromospheric waves that were previously thought to originate from the photosphere may be generated by some events in the chromosphere as well.

Keywords Chromosphere · Photosphere

1. Introduction

Recent research on the solar atmosphere has demonstrated complexities of the chromosphere, showing us that there is still a plethora of unexplained and previously unresolved

Initial Results from FISS
Guest Editor: Jongchul Chae

A. Anđić (✉)
Department of Astronomy, New Mexico State University, P.O. Box 3001, MSC 4500, Las Cruces, NM 88003, USA
e-mail: andic@astronomy.nmsu.edu

A. Anđić · K. Ahn · W. Cao
Big Bear Solar Observatory, 40386 North Shore Lane, Big Bear City, CA 92314, USA

J. Chae · H. Park · H. Yang · Y.D. Park
Astronomy Program, Department of Physics and Astronomy, Seoul National University, Seoul 151-741, Korea

dynamics there. Starting with Ellerman (1917) who noted a sudden bright event in the Hα line (Ellerman's bomb), the research so far has connected Ellerman bombs and K_{2V} brightenings to magnetic elements (Sivaraman and Livingston, 1982; Nindos and Zirin, 1998; Sivaraman *et al.*, 2000).

The complexity of the Ellerman bombs slowly emerged in the course of the research. Oscillatory signatures were observed in magnetic flux tubes by Volkmer, Kneer, and Bendlin (1995). From a theoretical standpoint Kalkofen (1997) interpreted intensity waves observed in the Ca II lines in terms of transverse and longitudinal magnetoacoustic waves propagating upward inside magnetic flux tubes. Successful models of Ca II grains, generated by acoustic shocks, were made by Carlsson and Stein (1992, 1997); they showed that bright Ca grains are produced primarily by waves from the photosphere whose frequency is slightly above the acoustic cut-off frequency. Connection between waves and brightening in the Ca bright points is also established and confirmed by observations; even later observations did not find any disagreement. Kariyappa, Narayanan, and Dame (2005) found that the chromospheric brightening observed in the Ca II H line is related to oscillations with a constant period (≈3 min), independent of their peak brightness.

Kalkofen (1999) proposed transverse and longitudinal waves in the magnetic flux tubes as an explanation for the observed dynamics, while Noble, Musielak, and Ulmschneider (2003) indicated the existence of torsional magnetic tube waves in flux tubes. The latter study was followed up by Musielak and Ulmschneider (2003) who considered the generation of longitudinal tube waves by the non-linear mode coupling with transverse waves and reproduced the observed 3-min oscillations. Khomenko, Collados, and Felipe (2008) found that horizontal motions in a deep portion of the flux tube generate a slow magnetosonic mode and a surface mode. These modes are efficiently transformed into a slow acoustic mode in the atmosphere where the Afvén speed is lower than the sound speed. Such a transformed mode might propagate along the field lines and effectively deposit the energy of the oscillatory driver into the chromosphere. These waves were observed two years later (Anđić *et al.*, 2010). However, a complex role played by the magnetic field in the lower atmosphere still gives a plenty of research topics. De Moortel and Galsgaard (2006) investigated the magnetic reconnection driven by rotational footpoint motions. An observational case was reported by Jess *et al.* (2007) who found rotational movement of oscillation sites (which were identified with the footpoints of flux tubes) during microflaring events.

The subsequent research has uncovered complexity in the chromospheric waves. Bodo *et al.* (2001) found that the temperature difference in a plasma, either in the horizontal or vertical direction, is enough to change the direction of the upward propagating waves, making them propagate along curved paths. Rosenthal *et al.* (2002) found that waves in the magnetic field that is significantly inclined from the vertical direction tend to get reflected from the surface of varying altitude. Jain and Haber (2002) found that acoustic waves are suppressed by the magnetic field, and the amount of the suppression increases with the field strength. Moreover, Bogdan *et al.* (2003) demonstrated that wave propagation in the presence of the magnetic field is complex. Some waves come directly from the source while the other waves come from the magnetic canopy due to mode conversion. The propagation directions of individual wave trains are not co-aligned with each other nor with the observer's line of sight. Also the characteristics of the observed waves depend on the ratio of thermal to magnetic pressure of their environment. This trend seems to continue in recent research. Shelyag *et al.* (2009) indicated that the magnetic field perturbs and scatters acoustic waves and absorbs the acoustic power of a wave packet. Their model showed that a highly curved strong magnetic field also partially transforms the wave packet into the slow magnetosonic mode that propagates downwards.

All these research results so far indicate that there might be a possibility that not all of the Ca II grains are generated by acoustic shocks, especially the ones located near complex magnetic field topography. Moreover, there is indication that photospheric and chromospheric waves may be independently excited (Leibacher, Gouttebroze, and Stein, 1982). Also, recently Reardon *et al.* (2008) found that chromospheric turbulence is generated by the acoustic shocks that reach the appropriate height due to steep vertical density gradients and that non-linear shock processes produce the cascade of energy to higher frequencies.

In this work we present the observations of a chromospheric bright point and its connection to the photospheric dynamics. In Section 2 we present the data and explain analysis procedures. In Section 3 we present results; first introducing the events themselves and observed photospheric dynamics, then we analyze waves detected in both chromospheric events and in the photosphere. In Section 4 we discuss results and connect them to the previous work. In Section 5 we summarize the conclusions.

2. Data and Analysis

The observations were performed with the New Solar Telescope (NST) at Big Bear Solar Observatory (Goode *et al.*, 2010) on 12 July 2009, using two instruments. Seeing was average and the low order adaptive optics system was used.

Imaging data of a small pore at solar coordinates E450″ N248″ were obtained using the optical setup at the Nasmyth focus with the following components: a broad-band filter centered at an absorption band of TiO molecules (705.68 nm) with a 1 nm band pass. This filter has also a 1 nm leakage around 613 nm with 25 % of the transmission of the main transmission band. However, this does not jeopardize the interpretation of our observations. The transmission of the filter is broad and averages over the line and continuum contributions, making the signal only weakly dependent on the properties of individual spectral lines. This is desirable in our case since the TiO line is very weak in the quiet Sun. Hence, we can assume that the height of formation of the image data is very close to that of the continuum. The used detector was a PCO.2000 camera (Cao *et al.*, 2010). The data set covers the time sequence of half an hour with 120 bursts of exposure, each of which was composed of 100 frames. The exposure of individual frames was 1 ms, and the cadence between bursts was 15 s. The field of view (FOV) was 70″ × 70″. The achieved resolution by Dawes' limit is 0.09″.

Simultaneously we performed spectroscopic observations with the Fast Imaging Solar Spectrograph (FISS) (Chae *et al.*, 2010). FISS is a field-scanning slit spectrograph with a typical spectral resolution of 1.4×10^5 and a unique capability for simultaneous observations at Hα and Ca II 854 nm in the fast scanning mode. For the observations reported here we scanned the field of 16″ × 40″, achieving a temporal cadence of 18 s. This FOV was contained within the FOV of the TiO imaging data. FISS was scanning both lines simultaneously with the spatial sampling of 0.16″. The angular resolution was determined by the seeing condition and is estimated to be about 1″. The images from the two instruments were co-aligned using a small pore in the FOV, since the resolution of the FISS instrument does not reveal the same detail in the photosphere as the TiO-band images. The pore itself was 3″ away from the event.

The TiO data set was calibrated (corrected for dark frames and flat-fielded) and then speckle reconstructed based on the speckle masking method (von der Lühe, 1993). For this purpose we used the Kiepenheuer Institut Speckle Interferometry Package (Wöger, von der Lühe, and Reardon, 2008). The cadence of the reconstructed TiO data provided us with a

Nyquist frequency of 67 mHz. The reconstructed images were aligned by a cross-correlation technique using a Fourier-transform routine and squared mean absolute deviations to provide sub-pixel alignment accuracy. We did not perform sub-pixel image shifting to avoid the interpolation errors that are inevitable with the use of this technique.

FISS data sets were also corrected for dark frames and flat-fielded following the procedures described by Chae *et al.* (2010). Velocity maps were constructed from the FISS data set using two different methods; the center-of-gravity method (Janssen, 2003) and the bisector method (Andjic, 2006; Andić, 2007a, 2007b). For both methods the reference (zero) point of the velocity was the average value of the analyzed points in the spectral line over the whole data set.

A wavelet analysis of intensity and velocity data was performed using the Morlet wavelet with the code based on Torrence and Compo (1998). An automated procedure was used here to carry out the wavelet analysis, as has been carried out previously and presented in detail by Bloomfield *et al.* (2006), with the restrictions described in detail in Andić *et al.* (2010).

As Lites and Chipman (1979) established, in a pure acoustic wave the upward velocity is in phase with enhancements in pressure, temperature, and density. Therefore, the phase relationship between the velocity and intensity signals in a spectral line can give insight into the nature of the observed waves and propagation characteristics. We analyzed the phase coherence using the wavelet approach (Bloomfield *et al.*, 2004). The difference in power contained in a time series computed with the traditional Fourier analysis and the wavelet analysis is small. The Fourier analysis, without timing information, has similar confidence levels when compared to the wavelet analysis averaged over time. Since the phase relation between the wave packets can change in time, the Fourier analysis loses information on these changes due to lack of timing information. The major cause of this loss is the fact that the phase can take a negative value as well, while the power is always positive. This is one reason why the wavelet analysis was adopted in our analysis. Since for pure noise this procedure yields positive coherence, only results with a coherence above 0.6 are regarded as significant.

The phase difference and phase coherence were calculated using the intensity and velocity data of two spectral line cores obtained with FISS and using intensity signal from the TiO data set. The velocity data were obtained from the spectral line bisector shift (Andjic, 2006; Andić, 2007a, 2007b). This processing allowed us to calculate phase differences in velocity–velocity (V-V), velocity–intensity (V-I), and intensity–intensity (I-I) data. The phase differences were calculated using the same spatial location (*i.e.* the same pixel in the field of view). The V-V and I-I phase differences were derived from two different spectral lines, while the V-I phase differences were calculated from the same spectral line. Therefore, the V-V and I-I phase differences reflect the difference in formation height of the corresponding line cores (Hα and Ca II).

Since the TiO data have only intensity images, in order to estimate the oscillatory phase of waves a different method had to be used. We combined the Fourier and Hilbert transforms on the single data set (White and Cha, 1973). The resulting signal is a complex function; its real part is the original signal and its imaginary part is a quadrature of the original signal. Since a real function and its quadrature are Hilbert transform pairs, the Hilbert transform converts one into another. The resulting transform describes the amplitude and phase of a variable in the complex plane. The signal is transformed into the Fourier space then transformed back using the Hilbert transform (Stebbins and Goode, 1987).

3. Results

We observed a brightening in the Ca II 854 nm line. In the vicinity of the brightening area, on a granular scale distance, we observed strong downflow in the Hα 656.28 nm line. The Ca II brightening and the Hα downflow areas were separated by about 3″. The events appeared simultaneously in Ca II 854 nm (Figure 1B) and Hα (Figure 1C), but at different locations. The events in both lines lasted for about 3 min. Prior to the Ca II brightening, we observed motions of resolved bright points (BPs) in the lower photosphere directly below the brightening area. These motions appeared at 8 min from the beginning of our time series and lasted until 12 min.

3.1. Line Profiles and Velocities

The velocity maps were obtained for both lines. For the Hα line, velocity maps were made from the wavelengths at the center of the line (656.28 nm), blue wing (656.21 nm), red wing (656.21 nm), blue continuum (655.9 nm), and red continuum (656.69 nm). For the Ca II line they were made from the wavelengths at the line center (854.21 nm), blue wing (854.17 nm), red wing (854.25 nm), blue continuum (853.65 nm), and red continuum (854.73 nm). The velocity maps revealed that the event in Hα was connected with strong downflow of plasma, while the brightening in Ca II with strong plasma upflow.

Figure 1C represents a strong downflow event observed in the velocity maps of Hα at spatial coordinates (5.6″, 4.1″). The duration of the event was determined by intensity changes in the area. The velocity signal at this location showed constant downflow, with its maximum velocity appearing ≈0.5 minute after the intensity showed the minimum value. The Hα spectral line profiles of this event show a red shift indicating velocities of about 5 km s^{-1} (Figure 2). The intensity at the red wing is 16 % higher than the one at the blue wing, indicating downflow. At the location of the Ca II event, downflow was observed in the Hα as well.

The simultaneous event in the Ca II line, separated from the Hα event by a spatial distance comparable to the granule size, showed indications of upflow (Figure 1B). The Ca II line profiles show a slight blue shift that corresponds to velocities of 2 km s^{-1} (Figure 3). The Ca II event is located at (1.4″, 2″) of the FOV. This event showed increases in velocity and intensity over the duration of the observation. The velocities measured at the wings were 30 % slower than the velocities observed at the line core. The Ca II velocity maps made from the line core and the blue wing both show the downflow at the location of the Hα event, which indicated that the same event was visible in both lines.

3.2. Photospheric Dynamics Under the Hα Event

Previous researches have indicated connections between Ca II brightening and magnetic elements (Sivaraman and Livingston, 1982; Nindos and Zirin, 1998; Sivaraman *et al.*, 2000). Our present analysis, on the contrary, suggests a possible connection between this chromospheric event and the dynamics of BPs in the photosphere (Figure 1A). In the following we describe the observed motions of small structures in the photosphere that were located below the corresponding chromospheric events.

In order to study the dynamics of BPs in the photosphere below the Hα event, we have selected a subregion of 3″ × 3″ in the TiO images. The Hα spectral data indicate downflow in this area, with its speed increasing throughout the observing run. This behavior in the Hα data suggests that the Hα downflow event might be associated with pronounced intergranular lanes in the TiO images at the same location, in view of the fact that intergranular lanes

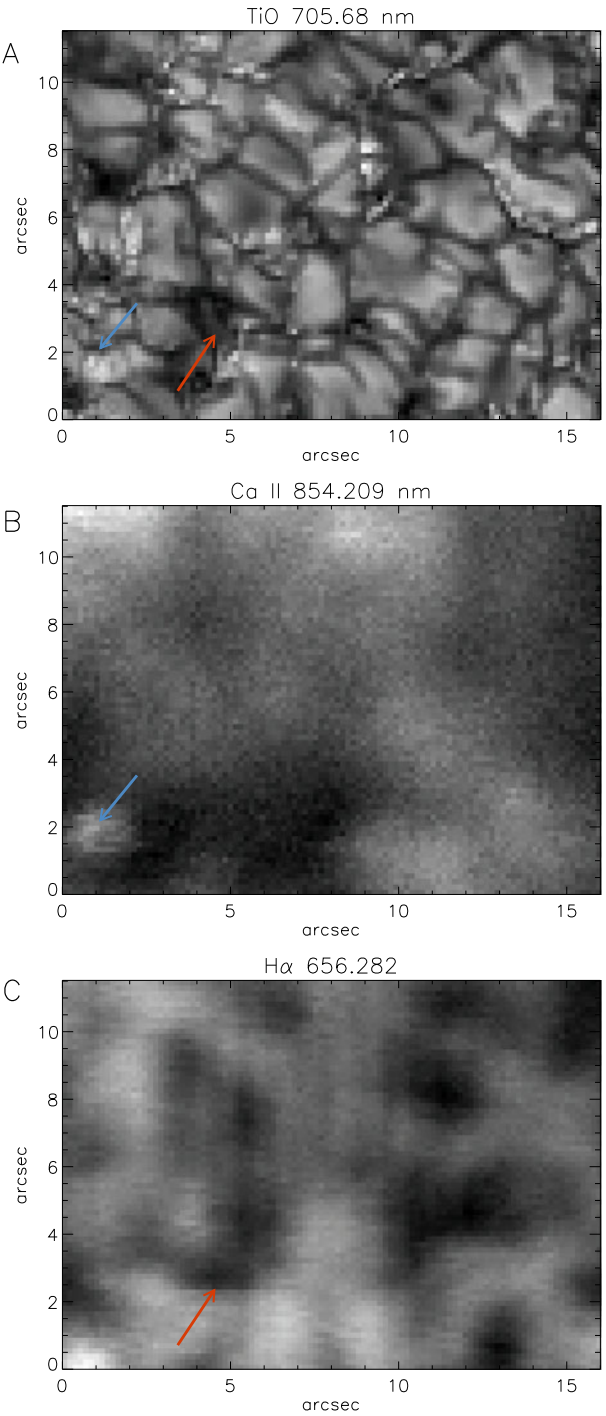

Figure 1 Observed events and corresponding photospheric configuration. Panel A is an image taken with a broad-band filter centered at the TiO band (705.68 nm). Arrows in panel A indicate small structures related to the event under consideration. The red and the blue arrows point to the locations of the Hα event and of the Ca II event, respectively. Panel B represents a core intensity image of the Ca II line 9 min from the beginning of the time series with the blue arrow marking the event, in this case brightening. Panel C is an Hα line core intensity image at the same moment as the peak intensity of the Ca II event. The red arrow points to the darkening event seen in this frame. Panels B and C were obtained by the FISS instrument.

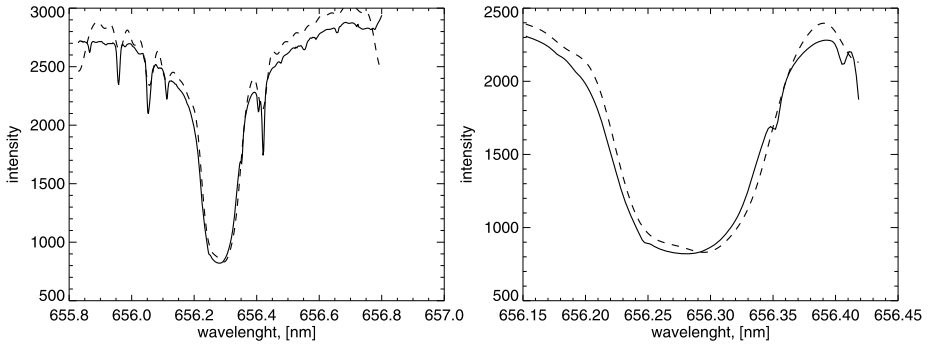

Figure 2 Hα line profiles of the Hα event. The left panel shows the full profile, while the right panel shows its enlarged line core. Solid lines represent a reference profile obtained by averaging the profiles over the whole field of view (FOV). Dashed lines are example profiles from the event. Noise in the profiles was filtered out with a low pass Fourier filter. A red shift corresponding to 6 km s^{-1} is seen.

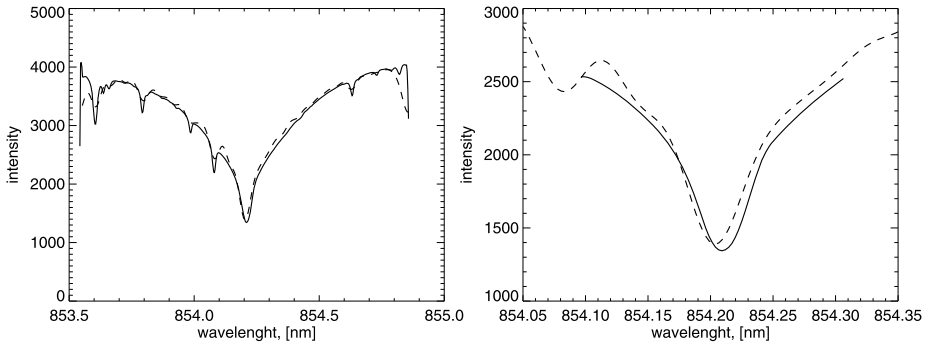

Figure 3 Ca II line profile of the Ca II event. The left panel shows the full profile, while the right panel shows its enlarged line core. Solid lines represent a reference profile obtained by averaging the profiles over the whole FOV. Dashed lines are example profiles from the event. Noise in the profiles was filtered out using a low pass Fourier filter. A blue shift corresponding to 2 km s^{-1} is seen.

are the places of persistent photospheric downflow. In fact, such an intergranular lane was observed as shown in Figure 4. A very broad lane started to form at 2 min after the beginning of the time series, and lasted till 5.5 min, when it contracted to a size typical of intergranular lanes. This continued presence of the intergranular lane during the Hα downflow event indicates a potential connection between chromospheric and photospheric dynamics.

In this intergranular lane we identified five BPs, and tracked them using the NAVE method (Chae and Sakurai, 2008) across the FOV of the subregion. As shown in Figure 5, the path of each BP neither crossed nor got closer to others' paths during the observing duration. This clear separation of the paths indicates that the motions of these BPs did not involve any flux tube entanglement at the photospheric level.

3.3. Photospheric Dynamics Under the Ca II Event

The photosphere below the Ca II brightening event showed different characteristics (Figure 6). In this location 21 BPs were identified and the majority of them were visible throughout the whole time series. But six of them were short-lived and ended their existence close

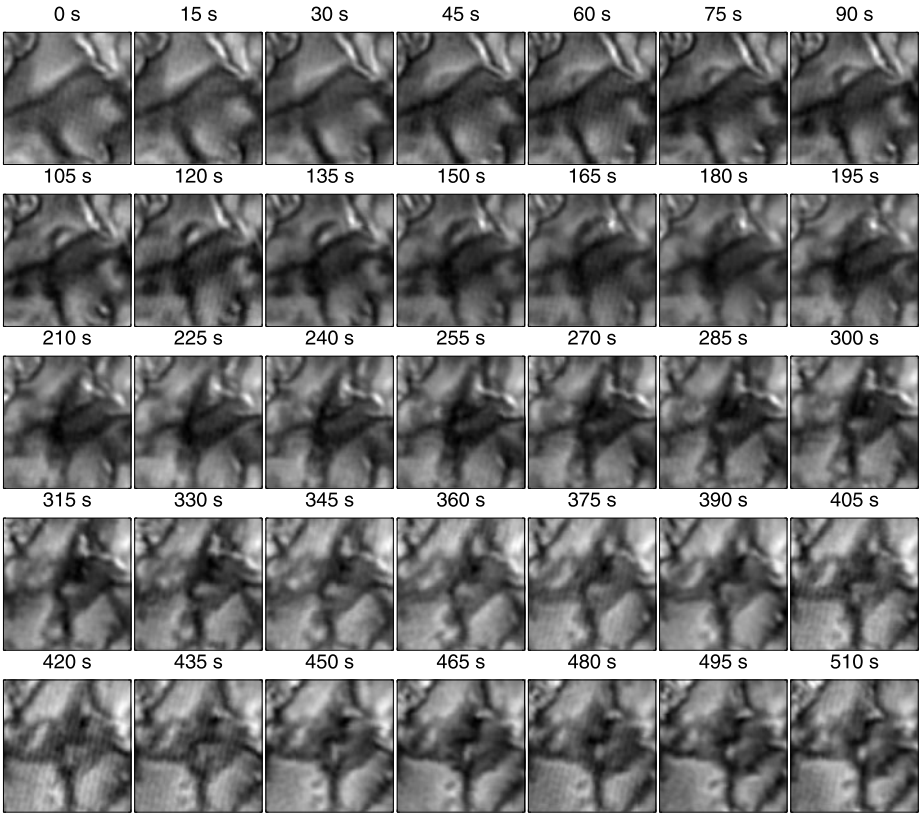

Figure 4 Time series of TiO filter images of the photosphere directly below the Hα event. Individual frame size is $3'' \times 3''$ and the time of observation measured from the beginning of the time series is shown above each frame.

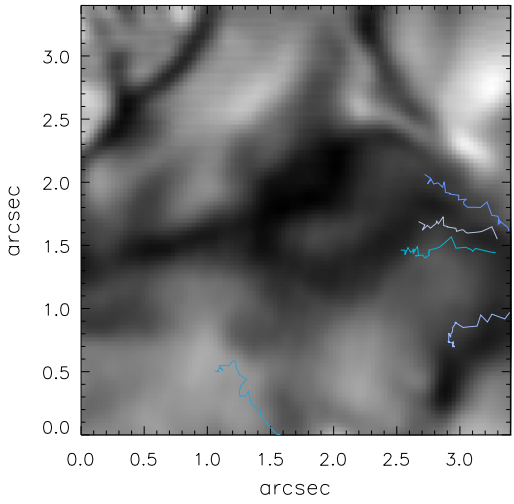

Figure 5 Average TiO-band image of the photosphere below the Hα event, taken by integrating over the first 10 min of the observing run. Colored lines in the frame represent the paths of five detected BPs during the observing run moving toward left.

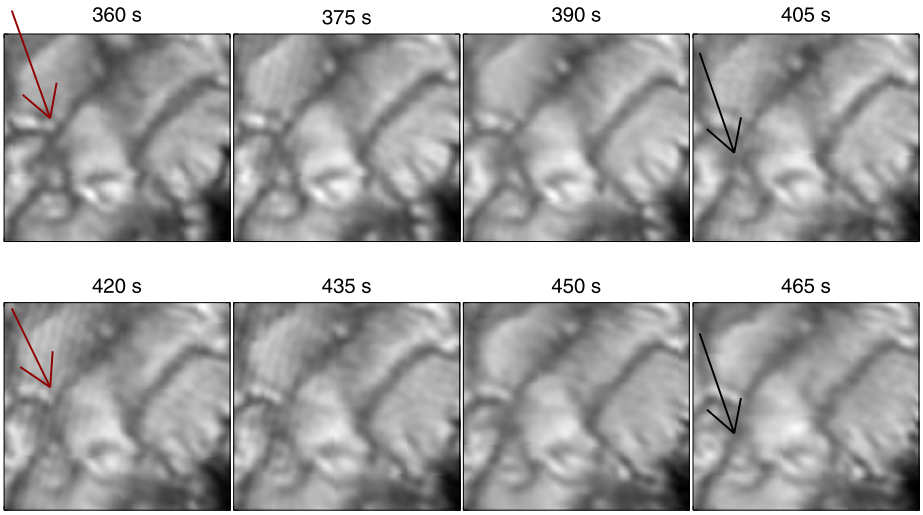

Figure 6 Time series of TiO filter images of the photosphere directly below the Ca II event. Individual frame size is $3'' \times 3''$. The arrows point to two pairs of BPs of our interest. The red arrows indicate one pair of BPs that was visible until 435 s, and the blue arrows indicate another pair of BPs that survived until 480 s.

Figure 7 Average TiO-band image of the photosphere below the Ca II event, taken by integrating over the first 10 min of the observational run. Colored curves in the frame represent the trajectories of six BPs moving towards left.

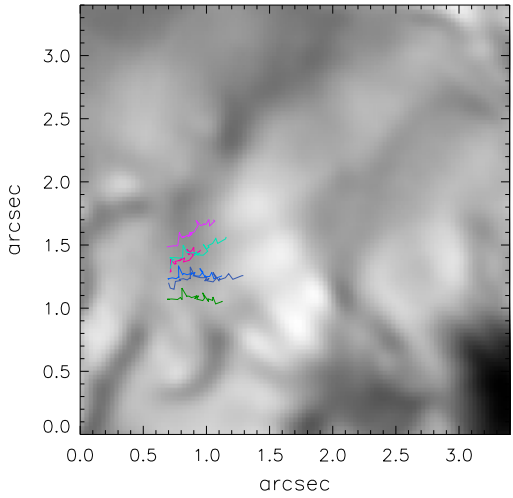

in time to the moment of maximum intensity and velocity amplitude of the Ca II upflow event. The disappearance occurred in pairs. One pair of BPs (as marked by the red arrows in Figure 6) ended their life at 6.75 min of the time series, and the other (as marked by the blue arrows) at 7.5 min. Moreover, we found that in each of these two pairs the two BPs were located so close to each other and crossed each other's path (Figure 7). This might indicate the entanglement of the flux tubes. These observed characteristics are quite consistent with the process of magnetic reconnection near the photosphere resulting in flux cancelation, mutual collision, and disappearance of two magnetic flux elements of opposite polarity.

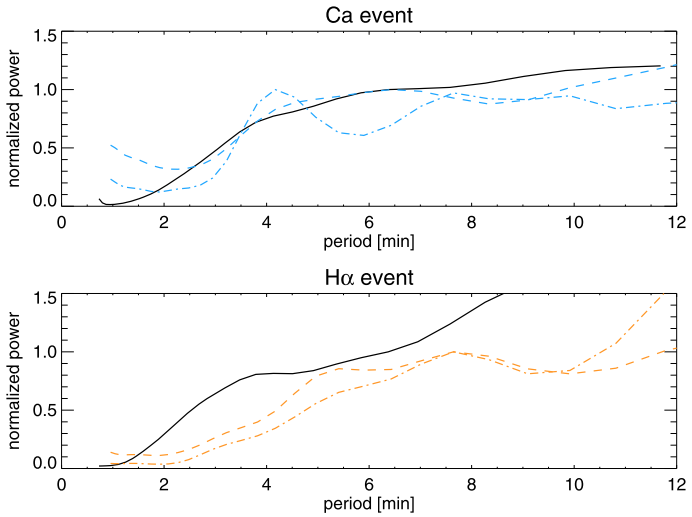

Figure 8 Top: Power spectra at the site of the Ca II event. The solid black curve represents the oscillatory power of TiO data, the dash-dotted blue curve shows the oscillatory power of Ca II intensity, and the blue dashed curve shows the power of Ca II velocity. Bottom: The same for the Hα event. The oscillatory power of TiO intensity is represented with the solid black curve, the oscillatory power of Hα intensity is shown with the dash-dotted orange curve, and the oscillatory power of Hα velocity is shown with the dashed orange curve.

3.4. Wavelet Analysis

We performed the wavelet analysis to detect waves connected with these events. For the TiO data set we analyzed intensity images, while for the Hα and Ca II data sets, we analyzed intensity and velocity data. We focus on the results of wavelet analysis at the locations and times of our events (Figure 8).

The figure shows that both events accompanied oscillation phenomena that may be considered as an observational manifestation of waves. The power spectrum of Ca II intensity in the Ca II event shows a strong peak at a period of $\approx$4 min. Two smaller peaks also appear at $\approx$7 and $\approx$10 min. In comparison, the power spectrum of TiO intensity data monotonically increases with period. The power spectrum of Hα intensity in the Hα event shows the most prominent peak at $\approx$7.5 min, and weak enhancement at $\approx$3 min. The power spectrum of velocity data has small peaks at 5 and 7.5 min. The power spectrum of TiO intensity increases with period like in the Ca II event, but has a small peak at $\approx$3.5 min.

3.5. Phase Differences

We analyzed phase differences between intensity and velocity (I-V) for the Hα and Ca II lines (Figure 9). The phase difference is set to zero if the peak brightening in the intensity signal occurs at the same time as the peak blueshift. According to a theory of the propagation of acoustic waves (Lites and Chipman, 1979), the upward velocity of an upward propagating acoustic wave should be in phase with the enhancements in pressure, temperature, density, and hence intensity. Thus, zero phase between intensity and velocity signal indicates upward propagation in an acoustic wave.

Figure 9 shows a complicated nature of the observed oscillations. The simplest wave trains are observed in the blue wings of both lines (Figures 9C and F), which may indicate

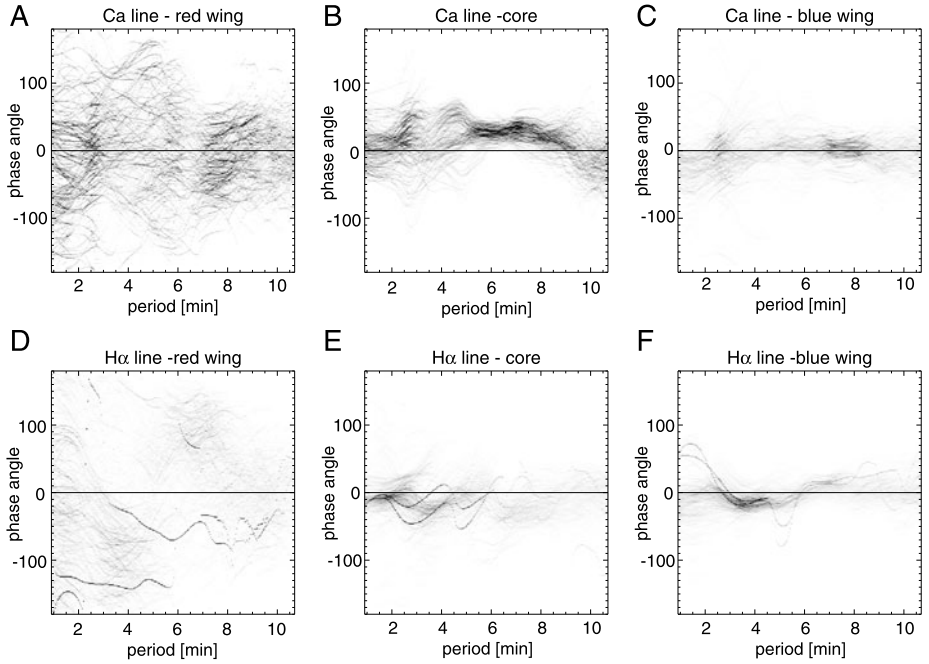

Figure 9 Top: Phase differences between intensity and velocity signals from the Ca II line. Panels A, B, and C are for red wing, line core, and blue wing, respectively. Bottom: Phase differences between intensity and velocity signals from the Hα line. Panels D, E, and F are for the red wing, line core, and blue wing, respectively.

acoustic wave trains. It appears, however, that the Ca II and Hα lines rather reflect the superposition of various wave modes. The most complicated wave trains are in the red wings of both lines (Figures 9A and D) where we see a plethora of different waves. The line cores (Figures 9B and E) also show mixture of different wave modes. These observed mixtures of phase differences suggest that in fact there may be more than one wave train, as predicted by Bogdan *et al.* (2003). Contributions from non-acoustics waves are also possible.

In Figure 10 we have presented phase differences between the Ca II line and the Hα line. The positive phase difference means that the Hα line signal follows that of the Ca II line. Since the Hα line is formed at a little higher level (1500 km above $\tau_{500\ \mathrm{nm}} = 1$; Vernazza, Avrett, and Loeser, 1981) than the Ca II line (1200 km; Cauzzi *et al.*, 2008), the phase difference between these lines is expected to be small and positive for upward propagating waves. But the V-V signals for either event do not show any clear signature of such expectation, only indicating a complex mixture of wave trains propagating in any direction with any speed (Figures 10B and D). Intensity phase differences in the Hα event show a similar situation (Figure 10C), namely a mixture of phase angles as V-V signals. Only the intensity phase differences found in the Ca II event show clear indication of positive phase differences in the period range from 4 to 6.5 min (Figure 10A). The detected positive phase difference means that the intensity signal first appears in the core of the Ca II line and then in the core of the Hα line. However, the difference between the formation heights of these two spectral lines is too small to explain these large phase differences in terms of simple upward propagating waves.

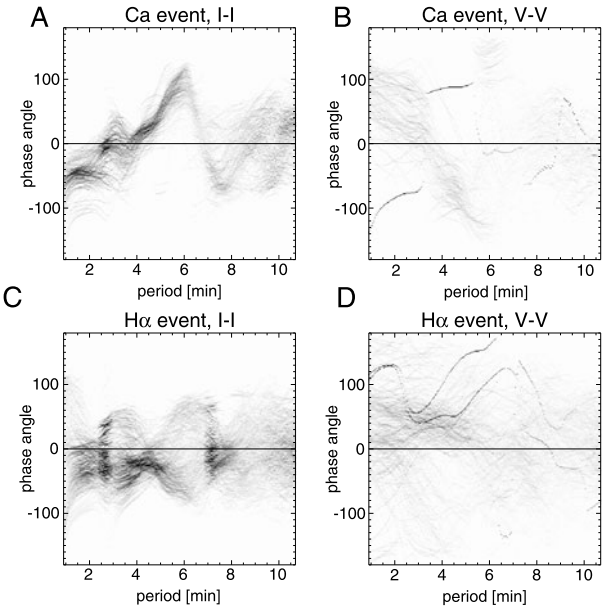

Figure 10 Phase differences for the Ca II (top) and Hα (bottom) events. Phase differences between Ca II and Hα lines are derived from intensity signals (left) and velocity signals (right), respectively. Positive phase difference means that a signal first appears in the Ca II line and then in the Hα line.

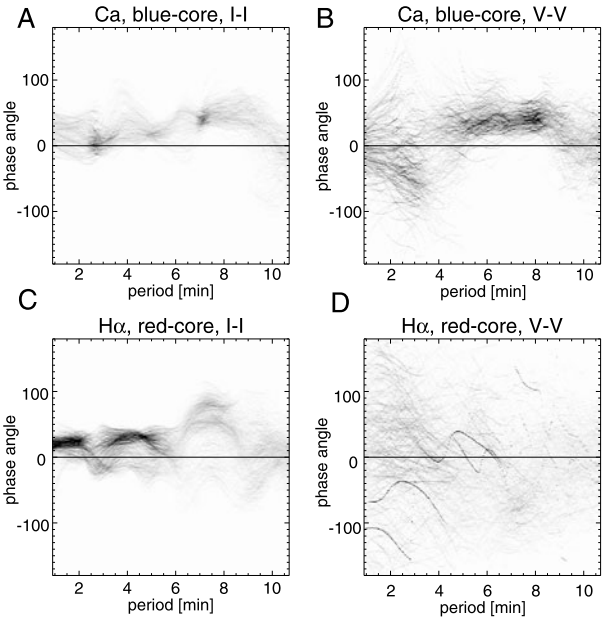

Figure 11 Phase differences for the Ca II (top) and Hα (bottom) events. Phase differences are derived from (A) blue wing and line core intensities of Ca II, (B) blue wing and line core velocities of Ca II, (C) red wing and line core intensities of Hα, and (D) red wing and line core velocities of Hα, respectively. Positive phase difference means that a signal first appears in the wing and then in the core of the line.

Since we detected the upflow from the Ca II line and the downflow from the Hα line in the velocity maps, we also examined any propagation of signals from the blue wing to the line core of the Ca II line and from the red wing to the line core of the Hα line (Figure 11). For the upflow event we have a clear propagation signature from the blue wing to the core in intensity and velocity signals (Figures 11A and B). The intensity signals show propagation

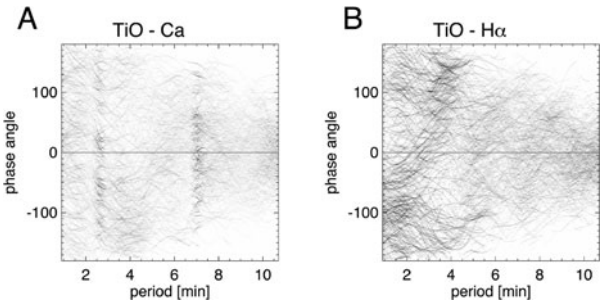

Figure 12 Phase differences between (A) TiO and Ca II intensities and (B) TiO and Hα intensities, respectively. Positive phase difference means that a signal first appears in the TiO line and then in the Ca II or Hα line.

from the wing to the core approximately over the whole period range (Figure 11A), while the velocity signals show clear propagation only in a period range of 5 to 9 min (Figure 11B).

The downflow event in Hα shows a different situation. In the intensity signals we see propagation from the red wing to the line core (Figure 11C) while the velocity signals show a chaotic mixture of waves moving in every direction with every speed (Figure 11D).

Previous researches suggested that Ca II brightening is caused by waves emitted from the photosphere. We tested this connection between the chromospheric events (Ca II and Hα) and photospheric waves (TiO) using their phase differences (Figure 12). In Figure 12 positive phase difference means that a signal first appears in TiO and then in Ca II or Hα. It is found that waves propagate simultaneously in upward and downward directions with various phase differences, and no clear trends are visible. Namely, the observed waves do not show any direct connection between the observed chromospheric events and photospheric dynamics below them.

Note that the phase differences shown in Figures 9, 10, 11, and 12 are weighted with power of the observed waves, making more powerful waves appear darker in the plots. Figure 12A shows that approximately all phase angles have some power, but we see a darker pattern appearing at periods ≈ 3 and ≈ 7 min. The concentrations of power near ≈ 3 min may indicate dominance of downward propagation (negative phase difference) while those near ≈ 7 min propagate in both directions, upward and downward. Figure 12B also shows concentrations of power in the Hα downflow event. In this case we see concentrations of power in the upward propagation with various phase angles in a period of ≈ 3.5 min and also in the downward propagation in the period range from 0.6 to ≈ 3.5 min.

3.6. Fourier–Hilbert Analysis

We applied the Fourier–Hilbert method to the TiO data to learn more about photospheric waves and their propagation direction. To make results comparable to the results of previous work, the amplitude and phase were integrated over the whole observing time, and were normalized with respect to their maximum value (Lites and Chipman, 1979). Then we removed all waves with amplitudes lower than 5 % of the maximum amplitude. In Figure 13 the amplitudes and phases thus derived are shown. The phase differences were presented in a weighted diagram, where the weight was applied by utilizing a cross-power amplitude $\sqrt{P_1 P_2}$. Here positive phase means upward propagating waves. For the Ca II event, where the BPs were located at around (1″, 1.2″), we see intense downward propagation of observed waves (Figure 13C). For the Hα event the situation is different; in the area where the intergranular lane was broadened we see strong upward propagation of the waves (Figure 13D).

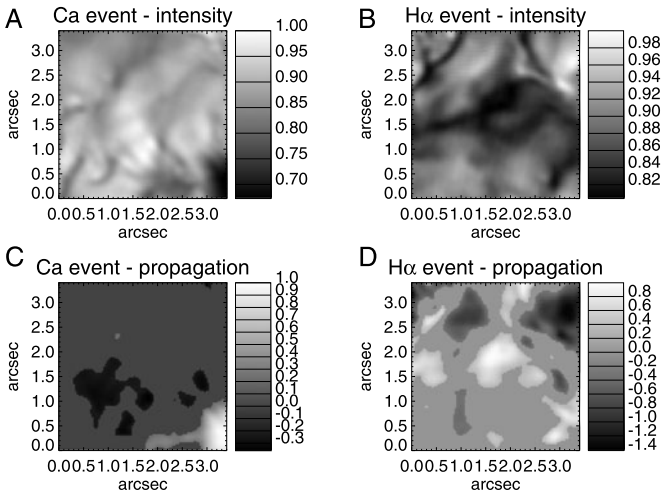

Figure 13 Normalized amplitudes (top) and phases (bottom) derived from the Fourier–Hilbert method applied to the TiO data. The left and right panels are for the Ca II and Hα events, respectively. The phase and amplitude were integrated over the observing time and normalized with respect to their maximum positive values. Then we removed all waves with amplitudes lower than 5 % of the maximum amplitude.

4. Discussion

We observed a Ca II brightening in one part of the FOV (Figure 3) with a strong upflow. In its vicinity we detected simultaneous strong downflow in the Hα line (Figure 2). The photosphere below the brightening area showed indications of possible flux tube entanglement (Figure 7), while at the location of the downflow we observed enhanced intergranular lanes (Figure 4). At a first glance it seems that the behavior of the photosphere corresponded to the observed events in the chromosphere.

Researchers in the past found that Ca II brightening events are related to magnetic elements (Sivaraman and Livingston, 1982; Sivaraman *et al.*, 2000), while brightening events in Hα or Ellerman bombs are not so, usually (Nindos and Zirin, 1998). Our findings agree with this work. We observed a Ca II brightening event above a cluster of BPs, without the accompanying Ellerman bombs (Figures 3 and 7). The location and intensity changes of the observed Ca II brightening fit the results of previous studies (Sivaraman and Livingston, 1982; Sivaraman *et al.*, 2000).

Kariyappa, Narayanan, and Dame (2005) observed the 3 min period waves in the Ca II brightening and speculated that they are due to chromospheric oscillations. Our work is in agreement with this speculation. Carlsson and Stein (1992, 1997) simulated the generation of Ca II brightening with acoustic shocks. However, we did not see this connection in our event.

Bogdan *et al.* (2003) pointed out that the location of the magnetic canopy and the location of the wave sources with their dominant state of polarization (radial vs. transverse driving motions) are important factors in considering the properties of propagating waves. The existence of a pore inside the FOV shows that parts of the canopy touched the photosphere inside the FOV, setting the canopy lower than in a typical quiet sun. Moreover, our FOV was close to the active region, AR 11087, which complicated the situation further. Our two spectral lines, Ca II and Hα, are formed in the height range of the canopy itself. Since we studied the wings and the centers of the lines, we can state that FISS data sets covered

significant portions of the canopy, but it is hard to say which portions exactly they did. Even from the simple quiet sun model by Vernazza, Avrett, and Loeser (1981) we see that the Ca II and Hα lines cover a wide range of atmospheric heights. Since inside the canopy the plasma conditions vary from one flux tube to the next it is hard to establish the exact range of spectral line formation. Thus, the closest we can state with certainty is that the Ca II and Hα lines are formed in the canopy. With the TiO-band observations the situation is clearer, data give information on the low photosphere.

We started our analysis with the assumption that the sources are located in the photosphere in the intergranular lanes, which is a typical situation for photospheric waves. The assumption was partially correct, as seen in Figure 13, but it did not provide the full answer since the phase differences between photospheric (TiO band) and chromospheric data did not agree with this picture (Figure 12).

Instead, the waves observed in the event are complex and point to a more than one oscillatory source being involved. The previous work established the existence of propagating waves in the flux tubes (DePontieu, Erdélýi, and James, 2004; Jess *et al.*, 2007; Andić *et al.*, 2010). Thus, one could expect to observe the wave propagation between photospheric and chromospheric layers especially when we observe along the axis of a flux tube. According to Bogdan *et al.* (2003) the propagation of the waves could be complex especially when the magnetic canopy is located in a part of the propagating path. Bogdan *et al.* (2003) found that the canopy area in the propagating path shows a very complex wave behavior in which fast waves are expected to propagate in a wide range of directions, especially in the direction close to the tangent of the magnetic loops. The complexity of our phase difference spectra shown in Figure 12 could be explained with the presence of a similar condition somewhere between the formation heights of the TiO band and the Ca II and Hα lines.

Most of the observed waves in Ca II and Hα during these two events show that they are not pure acoustic propagating waves (Figure 9), since for the acoustic waves one expect the brightening (intensity increase) to be in phase with the velocity of upflow (Lites and Chipman, 1979). The nature of the waves also confirms that they originate from additional sources, not only from the previously established photospheric sources which are thought to produce mainly acoustic waves (Nordlund and Stein, 2001; Khomenko, Collados, and Felipe, 2008; Andić *et al.*, 2010). Thus we can conclude that the upflow event is not connected with the waves created in the photosphere directly below it, but has a different origin.

From Figure 11 we see that there is a propagation of signals from the wings to the core of the line for the Ca II brightening event. But there was no such propagation between the photosphere and the Ca II formation height (Figure 12). Thus we might speculate that those propagating waves observed in the Ca II line most likely originate from the same mechanism as the observed upflow (Figure 3), and that complex propagation characteristics seen between the formation layers of the TiO band and of the Ca II line is partly caused by the same source emitting waves in all directions.

On the other hand, it is possible that waves observed in the chromosphere come from somewhere else via one of the many flux tubes that are intervened in the area. Unfortunately, due to our limited data sets without magnetic field information, we are not able to reconstruct the possible shapes and positions of the flux tubes, and consequently other possible candidates for the oscillatory sources in the photosphere are not excluded.

The downflow event observed in Hα was simultaneous with the upflow observed in Ca II, which made us believe that due to the simultaneous nature of the events and their closeness they are connected. However, we found no proof that those events are connected. The simultaneous changes in intensity of both events are most probably coincidental. The event itself shows strong downflow of plasma (Figure 2) that coincided with the persistent presence of

the intergranular lanes in the photosphere below the event (Figure 4). This indicates that the plasma downflow noted in Hα might have continued down to the photosphere.

The properties of waves are more complicated for the downflow event. Figure 13 shows that on the location of the downflow we have an emission of the upward propagating waves. This is in agreement with the previous studies (Andić, 2007b; and references therein). However, by examining the direction of wave propagation between the photosphere and the Hα formation height we encountered a complicated situation (Figure 12) that the wave trains propagated in both directions with a multitude of phase angles. These results are similar to the complexities of wave propagation demonstrated by Bogdan *et al.* (2003). This hypothesis is supported by the assumed location of the canopy in our data set. Figure 9D, E, and F demonstrate that the waves observed in Hα are a mixture of various wave modes. Figure 11D shows that the complexity of wave propagation continued to the Hα line formation height. Figure 11C is the only phase spectrum that clearly shows a propagation from the red wing to the core of the Hα line. Even in this case a general impression is that the wave trains in the plasma in the downflow event are complex with multiple wave sources and wave modes and thus require more detailed data sets combined with theoretical modeling to fully understand what is going on with the waves during the plasma downflow of this kind.

5. Conclusions

We observed the Ca II brightening event that coincided with the plasma upflow and it was located above the magnetic elements in the photosphere. However, we could not observe the connection between the waves in the photosphere and those in the Ca II brightening area. We speculate that the waves in the brightening area are alternatively caused by magnetic reconnection that is most likely to have caused brightening itself and the plasma upflow. As Bogdan *et al.* (2003) demonstrated, the behavior of waves is complex in the canopy configuration, and observations of the photosphere and the lower chromosphere with instruments that allow 2D spectropolarimetry would be beneficial to investigate complicated processes going on in this height range.

In the case of the plasma downflow event, we found that upward propagating waves are created in the intergranular lanes. However, the propagation of the waves became complicated when the chromosphere is included into the analysis. Although it is possible that the plasma downflow continued from the Hα line formation height all the way down to the low photosphere, the nature of the propagating waves is not perfectly clear. It seems that multiple oscillatory sources and/or sites were involved where the waves might be reflected from the magnetic canopy and might change modes (Bogdan *et al.*, 2003). Unfortunately, this last part is only speculation, since the places of reflection and additional sources could not be identified in our data set.

Acknowledgements The authors are thankful to the anonymous referee for helpful comments. AA is thankful to J. Varsik and R. Fear for the help with the observations. K. Ahn and W. Cao acknowledge the support of the US NSF AGS-0847126. The work of J. Chae, H. Park, and H. Yang was supported by the National Research Foundation of Korea (KRF-2008-220-C00022), and that of Y.D. Park, by the Development of Korean Space Weather Center, a project of KASI.

References

Ahn, K., Chae, J., Park, H.M., Nah, J., Park, Y.D., Jang, B.H., Moon, Y.J.: 2008, *J. Korean Astron. Soc.* **41**, 39.

Andjic, A.: 2006, *Serb. Astron. J.* **172**, 27.
Andić, A.: 2007a, *Solar Phys.* **242**, 9.
Andić, A.: 2007b, *Solar Phys.* **243**, 131.
Andić, A., Goode, P.R., Chae, J., Cao, W., Ahn, K., Yurchyshyn, V., Abramenko, V.: 2010, *Astrophys. J. Lett.* **717**, L79.
Bloomfield, D.S., McAteer, R.T.J., Lites, B.W., Judge, P.G., Mathioudakis, M., Keenan, F.P.: 2004, *Astrophys. J.* **617**, 623.
Bloomfield, D.S., McAteer, R.T.J., Mathioudakis, M., Keenan, F.P.: 2006, *Astrophys. J.* **652**, 812.
Bodo, G., Kalkofen, W., Massaglia, S., Rossi, P.: 2001, *Astron. Astrophys.* **370**, 1088.
Bogdan, T.J., Carlsson, M., Hansteen, V., McMurry, A., Rosenthal, C.S., Jonson, M., Petty-Powell, S., Zita, E.J., Stein, R.F., McIntosh, S.W.: Nordlund, Å.: 2003, *Astrophys. J.* **599**, 626.
Cao, W., Gorceix, N., Coulter, R., Woeger, F., Ahn, K., Shumko, S., Varsik, J., Coulter, A., Goode, P.R.: 2010, In: McLean, I.S., Ramsay, S.K., Takami, H. (eds.) *Ground-Based and Airborne Instrumentation for Astronomy III*, *Proc. SPIE* **7735**, 77355V.
Cauzzi, G., Reardon, K.P., Uitenbroek, H., Cavallini, F., Falchi, A., Falciani, R., Janssen, K., Rimmele, T., Vecchio, A., Wöger, F.: 2008, *Astron. Astrophys.* **480**, 515.
Chae, J., Sakurai, T.: 2008, *Astrophys. J.* **689**, 593.
Chae, J., Goode, P.R., Ahn, K., Yurchycsyn, V., Abramenko, V., Andić, A., Cao, W., Park, Y.D.: 2010, *Astrophys. J. Lett.* **713**, L6.
Carlsson, M., Stein, R.R.: 1992, *Astrophys. J. Lett.* **397**, L59.
Carlsson, M., Stein, R.F.: 1997, *Astrophys. J.* **481**, 500.
De Moortel, I., Galsgaard, K.: 2006, *Astron. Astrophys.* **451**, 1101.
DePontieu, B., Erdélýi, R., James, S.P.: 2004, *Nature* **430**, 536.
Ellerman, F.: 1917, *Astrophys. J.* **46**, 298.
Goode, P.R., Yurchyshyn, V., Cao, W., Abramenko, V., Andić, A., Ahn, K., Chae, J.: 2010, *Astrophys. J. Lett.* **714**, L31.
Jain, R., Haber, D.: 2002, *Astron. Astrophys.* **387**, 1092.
Janssen, K.: 2003, *Struktur und Dynamik kleinskaliger Magnetfelder der Sonnenatmosphaere*, Copernikus GmbH, Kaltenburg-Lindau, 123.
Jess, D.B., McAteer, R.T.J., Mathioudakis, M., Keenan, F.P., Andić, A., Bloomfield, D.S.: 2007, *Astron. Astrophys.* **476**, 971.
Kalkofen, W.: 1999, In: Schmieder, B., Hofmann, A., Staude, J. (eds.) *Third Advances in Solar Physics Euroconference: Magnetic Fields and Oscillations*, *ASP Conf. Ser.* **184**, 227.
Kalkofen, W.: 1997, *Astrophys. J. Lett.* **486**, L145.
Kariyappa, R., Satya Narayanan, A., Damé, L.: 2005, *Bull. Astron. Soc. India* **33**, 19.
Khomenko, E., Collados, M., Felipe, T.: 2008, *Solar Phys.* **251**, 589.
Leibacher, J., Gouttebroze, P., Stein, R.F.: 1982, *Astrophys. J.* **258**, 393.
Lites, B.W., Chipman, E.G.: 1979, *Astrophys. J.* **231**, 570.
Musielak, Z.E., Ulmschneider, P.: 2003, *Astron. Astrophys.* **406**, 725.
Nindos, A., Zirin, H.: 1998, *Solar Phys.* **182**, 381.
Noble, M.W., Musielak, Z.E., Ulmschneider, P.: 2003, *Astron. Astrophys.* **409**, 1085.
Nordlund, Å., Stein, R.F.: 2001, *Astrophys. J.* **546**, 576.
Reardon, K.P., Leperti, F., Carbone, V., Vecchio, A.: 2008, *Astrophys. J. Lett.* **683**, L207.
Rosenthal, C.S., Bogdan, T.J., Carlsson, M., Dorch, S.B.F., Hansteen, V., McIntosh, S.W., McMurry, A., Nordlund, Å., Stein, R.F.: 2002, *Astrophys. J.* **564**, 508.
Shelyag, S., Zharkov, S., Fedun, V., Erdélyi, R., Thompson, M.J.: 2009, *Astron. Astrophys.* **501**, 735.
Sivaraman, K.R., Livingston, W.C.: 1982, *Solar Phys.* **80**, 227.
Sivaraman, K.R., Gupta, S.S., Livingston, W.C., Damé, L., Kalkofen, W., Keller, C.U., Smartt, R., Hasan, S.S.: 2000, *Astron. Astrophys.* **363**, 279.
Stebbins, R., Goode, P.R.: 1987, *Solar Phys.* **110**, 237.
Torrence, C., Compo, G.P.: 1998, *Bull. Am. Meteorol. Soc.* **79**, 61.
Vernazza, J.E., Avrett, E.H., Loeser, R.: 1981, *Astrophys. J. Suppl.* **45**, 635.
Volkmer, R., Kneer, F., Bendlin, C.: 1995, *Astron. Astrophys.* **304**, 1.
von der Lühe, O.: 1993, *Astron. Astrophys.* **268**, 347.
White, O.R., Cha, M.Y.: 1973, *Solar Phys.* **31**, 23.
Wöger, F., von der Lühe, O., Reardon, K.: 2008, *Astron. Astrophys.* **488**, 375.